



HAL
open science

Investigation of the Gas-Phase Reaction of Nopinone with OH Radicals: Experimental and Theoretical Study

Gisele El Dib, Mano Priya Angappan, Senthilkumar Lakshmipathi

► **To cite this version:**

Gisele El Dib, Mano Priya Angappan, Senthilkumar Lakshmipathi. Investigation of the Gas-Phase Reaction of Nopinone with OH Radicals: Experimental and Theoretical Study. *Atmosphere*, 2022, 13 (8), pp.1247. 10.3390/atmos13081247 . hal-03796698

HAL Id: hal-03796698

<https://hal.science/hal-03796698>

Submitted on 4 Oct 2022

HAL is a multi-disciplinary open access archive for the deposit and dissemination of scientific research documents, whether they are published or not. The documents may come from teaching and research institutions in France or abroad, or from public or private research centers.

L'archive ouverte pluridisciplinaire **HAL**, est destinée au dépôt et à la diffusion de documents scientifiques de niveau recherche, publiés ou non, émanant des établissements d'enseignement et de recherche français ou étrangers, des laboratoires publics ou privés.



Distributed under a Creative Commons Attribution 4.0 International License

Article

Investigation of the Gas-Phase Reaction of Nopinone with OH Radicals: Experimental and Theoretical Study

Gisèle El Dib ^{1,*} , Angappan Mano Priya ² and Senthilkumar Lakshmipathi ^{3,*} ¹ CNRS, IPR (Institut de Physique de Rennes)-UMR 6251, Université de Rennes, F-35000 Rennes, France² Department of Physics, PSGR Krishnammal College for Women, Coimbatore 004, India³ Department of Physics, Bharathiar University, Coimbatore 046, India

* Correspondence: gisele.eldib@univ-rennes1.fr (G.E.D.); lsenthilkumar@buc.edu.in (S.L.);

Tel.: +33-223-235-680 (G.E.D.); +94-43-702753 (S.L.)

Abstract: Monoterpenes are the most essential reactive biogenic volatile organic compounds. Their removal from the atmosphere leads to the formation of oxygenated compounds, such as nopinone (C₉H₁₄O), one of the most important first-generation β-pinene oxidation products that play a pivotal role in environmental and biological applications. In this study, experimental and theoretical rate coefficients were determined for the gas-phase reaction of nopinone with hydroxyl radicals (OH). The absolute rate coefficient was measured for the first time using a cryogenically cooled cell along with the pulsed laser photolysis–laser-induced fluorescence technique at 298 K and 7 Torr. The hydrogen abstraction pathways were found by using electronic structure calculations to determine the most favourable H-abstraction position. Pathway 5 (bridgehead position) was more favourable, with a small barrier height of −1.23 kcal/mol. The rate coefficients were calculated based on the canonical variational transition state theory with the small-curvature tunnelling method (CVT/SCT) as a function of temperature. The average experimental rate coefficient ($1.74 \times 10^{-11} \text{ cm}^3 \text{ molecule}^{-1} \text{ s}^{-1}$) was in good agreement with the theoretical value ($2.2 \times 10^{-11} \text{ cm}^3 \text{ molecule}^{-1} \text{ s}^{-1}$). Conclusively, the results of this study pave the way to understand the atmospheric chemistry of nopinone with OH radicals.

Keywords: nopinone; OH radical; abstraction mechanism; rate coefficient; atmospheric implications



Citation: El Dib, G.; Mano Priya, A.; Lakshmipathi, S. Investigation of the Gas-Phase Reaction of Nopinone with OH Radicals: Experimental and Theoretical Study. *Atmosphere* **2022**, *13*, 1247. <https://doi.org/10.3390/atmos13081247>

Academic Editors: Haichao Wang and Zhaofeng Tan

Received: 1 July 2022

Accepted: 4 August 2022

Published: 5 August 2022

Publisher's Note: MDPI stays neutral with regard to jurisdictional claims in published maps and institutional affiliations.



Copyright: © 2022 by the authors. Licensee MDPI, Basel, Switzerland. This article is an open access article distributed under the terms and conditions of the Creative Commons Attribution (CC BY) license (<https://creativecommons.org/licenses/by/4.0/>).

1. Introduction

Biogenic volatile organic compounds (BVOCs) account for approximately 90% of VOCs present in the atmosphere [1,2]. Monoterpenes (C₁₀H₁₆) are ubiquitous in the atmosphere and contribute around 11% of the total estimated BVOC emission flux globally [3,4]. In the atmosphere, monoterpenes may undergo a wide variety of chemical reactions with photooxidants and form first-generation β-pinene oxidation products, which are likely precursors of greenhouse gases (GHGs) and secondary organic aerosols (SOAs) [5]. Some of these first-generation β-pinene oxidation products have been observed in the atmosphere during field campaigns [6]. However, they were detected in small amounts, most likely due to their rapid elimination by atmospheric oxidants and photolysis reactions. In addition, the levels of SOA observed in field campaigns are often higher than those predicted by models, suggesting that these species may be potential sources of SOAs [7]. Although many studies exist on biogenic organic compounds emitted by vegetation, information on the atmospheric fate of the first-generation β-pinene oxidation products is scarce.

Among those oxidation products, nopinone (C₉H₁₄O) is one of the optimal β-pinene oxidation products for measurement in the atmosphere. Indeed, this product is considered a good gaseous tracer of the photo-oxidation of β-pinene, since it is formed in the atmosphere in large quantities during the oxidation of β-pinene by OH radicals (>25%) and O₃ (40%) [8,9]. In addition to its formation by the atmospheric oxidation of β-pinene,

the bubbler containing H_2O_2 in the liquid phase, and it was saturated with H_2O_2 vapour when exiting from the bubbler. A thermocouple was attached to the bubbler wall in order to measure the temperature in real time and thus to precisely determine the H_2O_2 and OH vapour pressures. The concentrations of H_2O_2 in the gas mixture in the reactor were calculated from the mass flow rates, the vapour pressure of H_2O_2 , the temperature and the pressure in the reactor and those in the bubbler. A mixture of 0.5% of nopinone vapour in 750 Torr of argon was prepared in a bulb with a known volume. This mixture was then introduced into the reactor, in which the concentration of nopinone was calculated from the temperature and the total pressure in the reactor, the mass flow rates and the mixture rate in the bulb.

The main carrier gas was introduced into the reactor 25 cm upstream of the detection zone. The mass flow rates were measured by using calibrated mass flow controllers from MKS (100–10,000 sccm). Two thermocouples positioned at the entrance of the gas and upstream of the detection zone were used to measure the temperature inside the reactor. The pressure was measured by using (10–1000 Torr) MKS capacitance manometers. OH radicals were generated in the ground state $X^2\Pi, v'' = 0$ by the photodissociation of H_2O_2 using the pulsed-laser photolysis (PLP) technique, where a photolysis beam emitted by a Nd:YAG laser at 266 nm passed longitudinally through the reactor to photodissociate H_2O_2 . The laser fluence was typically $30 \pm 1 \text{ mJ pulse}^{-1} \text{ cm}^{-2}$. The OH radical concentration at the initial time was calculated according to the following equation:

$$[\text{OH}]_0 = 5 \times 10^{12} \times \lambda \times F_l \times \sigma \times \varphi \times [\text{H}_2\text{O}_2] \quad (1)$$

where λ is the wavelength (266 nm), F_l is the energy fluence of the photolysis laser (mJ cm^{-2}), σ is the absorption cross-section of H_2O_2 at 265 nm, $\varphi = 2$ is the quantum yield of the photodissociation of H_2O_2 and $[\text{H}_2\text{O}_2]$ is the concentration of H_2O_2 introduced into the reactor.

The laser-induced fluorescence (LIF) technique was used to monitor the temporal OH decay due to its reaction with nopinone. A frequency-doubled dye laser (Continuum ND 6000) pumped by a Nd:YAG laser (Spectra Physics, GCR 230) emitting at 532 nm was used as the probe laser. This later crossed perpendicularly with the photolysis beam through the reactor to excite the OH radicals at 281.99 nm (electronic transition $A^2\Sigma^+ - X^2\Pi (1,0)$). A photomultiplier tube (PMT) positioned in the middle of the reactor perpendicular to both the laser beams and gas flows was used to detect the OH fluorescence (transition $A^2\Sigma^+ - X^2\Pi (1,1)$ and $(0,0)$ at ca. 310 nm). The output pulse of the PMT was then integrated for a pre-set period by a gated charge integrator. Both the photolysis and the fluorescence lasers had repetition rates of 10 Hz.

The OH decay was determined according to the following relation:

$$[\text{OH}] = [\text{OH}]_0 e^{-k_{first} t} \quad (2)$$

with

$$k_{first} = k [\text{nopinone}] \quad (3)$$

where t is the delay time between photolysis and the probe beams, $[\text{OH}]_0$ and $[\text{OH}]$ are the concentrations of OH at the initial time and at time t , respectively, k_{first} is the first-order rate coefficient and k is the rate coefficient for the reaction of nopinone with OH radicals. Typically, 10 fluorescence decays were averaged to generate OH concentration vs. time profiles (see Figure 1).

The rate coefficient was determined under pseudo-first-order conditions, where the concentration of nopinone was in large excess compared to that of OH. Experiments were carried out under flow conditions, where the gas mixture was renewed between two consecutive photolysis pulses to avoid the accumulation of photolysis or reaction products. Table 1 summarizes the experimental conditions used during this study.

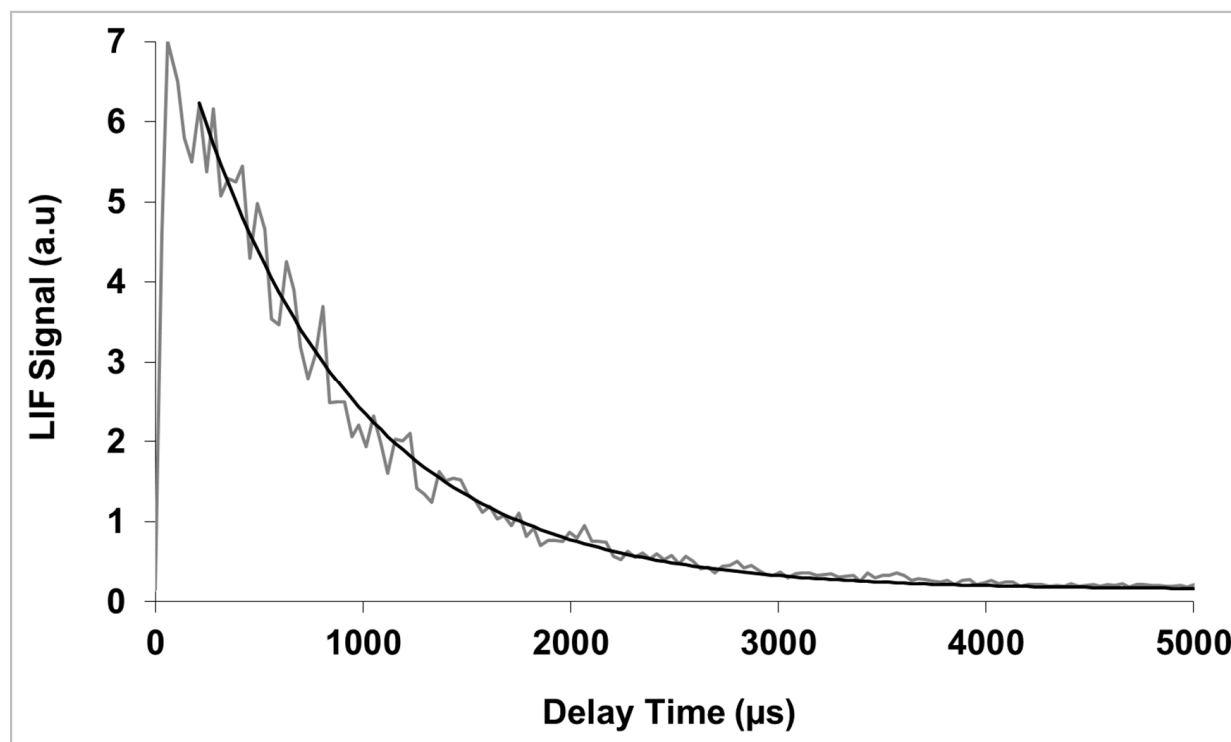


Figure 1. Decay of the LIF signal as a function of the delay time between the pulses from the photolysis and probe lasers. $P = 80$ Torr; $T = 298$ K; $[\text{OH}]_0 = 11 \times 10^{11}$ radicals cm^{-3} ; buffer gas: argon.

Table 1. Experimental conditions and rate coefficients obtained experimentally at 298 K and under a pressure range of 7 to 80 Torr in argon.

Pressure /Torr	Linear Velocity / cm s^{-1}	$[\text{OH}]_0$ / 10^{11} radical cm^{-3}	$[\text{nopinone}]$ / 10^{14} molecule cm^{-3}	k / 10^{-11} cm^3 molecule $^{-1}$ s^{-1}
7	370	9	0.30–4.35	1.75 ± 0.35
20	320	11	0.44–4.35	1.79 ± 0.35
20	320	11	0.70–4.25	1.69 ± 0.35
80	248	11	0.30–4.65	1.73 ± 0.35
				1.74 ± 0.35^a

^a The uncertainty of the average value was calculated according to this equation: $\sigma_{\text{average}} = \frac{1}{\sqrt{\sum_{i=1}^n (1/\sigma_i^2)}}$.

The chemicals used in this work were provided by Sigma Aldrich. Nopinone (purity > 95%) was purified by repeated freeze–pump–thaw cycles before use. The final purity was equal to 97%. The H_2O_2 solution (50% in water) was concentrated by bubbling argon through the solution to remove water for several days prior to use. Argon > 99.995% was provided by Air Liquid.

2.2. Computational Details

The abstraction reaction mechanism of nopinone with OH radicals was theoretically studied to support and analyse the experimental results. The geometries of the stationary points involved in the hydrogen abstraction reaction of nopinone with OH radicals were determined using the density functional theory (DFT) method at the M06-2X/6-311++G(d,p) basis set. Previous studies [16–19] have reported that this level of theory provides accurate results for atmospheric reactions and kinetics calculations. Vibrational analysis was carried

out at the same level of theory, and the transition state structures were characterized with one imaginary frequency; these structures corresponded to first-order saddle points. Intrinsic reaction co-ordinate (IRC) calculations were performed to confirm the reaction energy paths [20,21]. In addition to reaction energy barrier calculations, the rate coefficient of the reaction was calculated using the canonical variational transition state theory (CVT) with a small-curvature tunnelling method [22–24]. The rate coefficient at temperature T is given by the following relationship [22,23]:

$$k^{CVT}(T) = \min_s k^{GT}(T, s) \quad (4)$$

where

$$k^{GT}(T, s) = \frac{\sigma k_B T}{h} \frac{Q^{GT}(T, s)}{\phi^R(T)} \exp\left(\frac{-v_{MEP(s)}}{k_B T}\right) \quad (5)$$

where \min_s signifies the location of the generalized transition state (GTS) at the minimized dividing surface s , $k^{GT}(T, s)$ is the generalized transition state (GTS) theory rate constant at the dividing surface s , σ is the symmetry factor to illustrate the possibility of more than one symmetry-related reaction path, k_B is Boltzmann's constant, h is Planck's constant, $\phi^R(T)$ is the reactant classical partition function per unit volume, $Q^{GT}(T, s)$ is the classical partition function of a GTS with a local zero of energy $v_{MEP(s)}$ and with all rotational symmetry numbers set to unity, $v_{MEP(s)}$ is the classical potential energy at point s on the minimum energy path.

The kinetics of all reaction pathways were calculated using the GAUSSRATE 2009A [22] program, an interface between the GAUSSIAN09 and POLYRATE 2010A [25] programs. All of the electronic structure calculations were performed using the GAUSSIAN09 [26] program.

3. Results and Discussion

3.1. Experimental Kinetic Study

The results obtained experimentally are summarized in Table 1. All rate coefficients were measured at 298 K and under a pressure range of 7 to 80 Torr in argon. As shown in Table 1, the variation in the total pressure from 7 to 80 Torr had no effect on the rate coefficients within the experimental errors.

An example of a plot of the pseudo-first-order decay rates as a function of the nopinone concentration is shown in Figure 2. The slope of the straight line is the second-order rate coefficient according to Equation (3). Each individual second-rate coefficient presented in Table 1 is the average resulting from three runs conducted under the same conditions. The uncertainties in these values were estimated at around 20%, and they came from both statistical and systematic errors. The statistical errors originated from the least-squares analysis of the plot of k_{first} vs. [nopinone] displayed in Figure 2, multiplied by the Student's t -factor appropriate for the 95% confidence interval and the number of degrees of freedom. The systematic errors are mainly due to difficulty handling nopinone, given its low volatility.

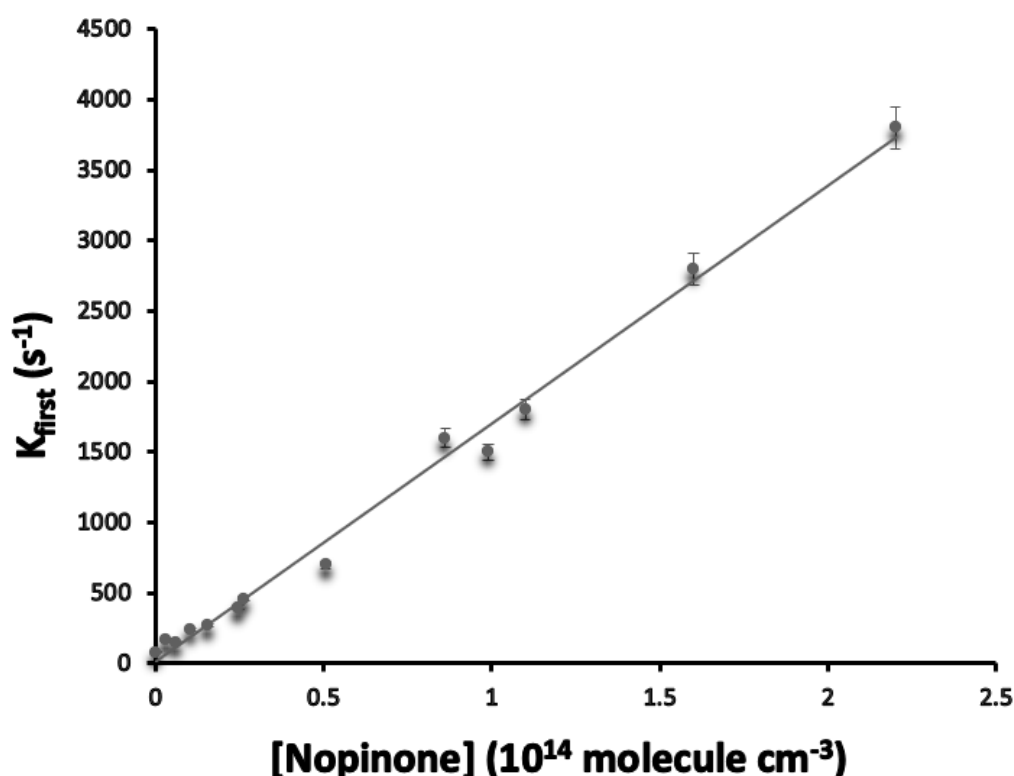
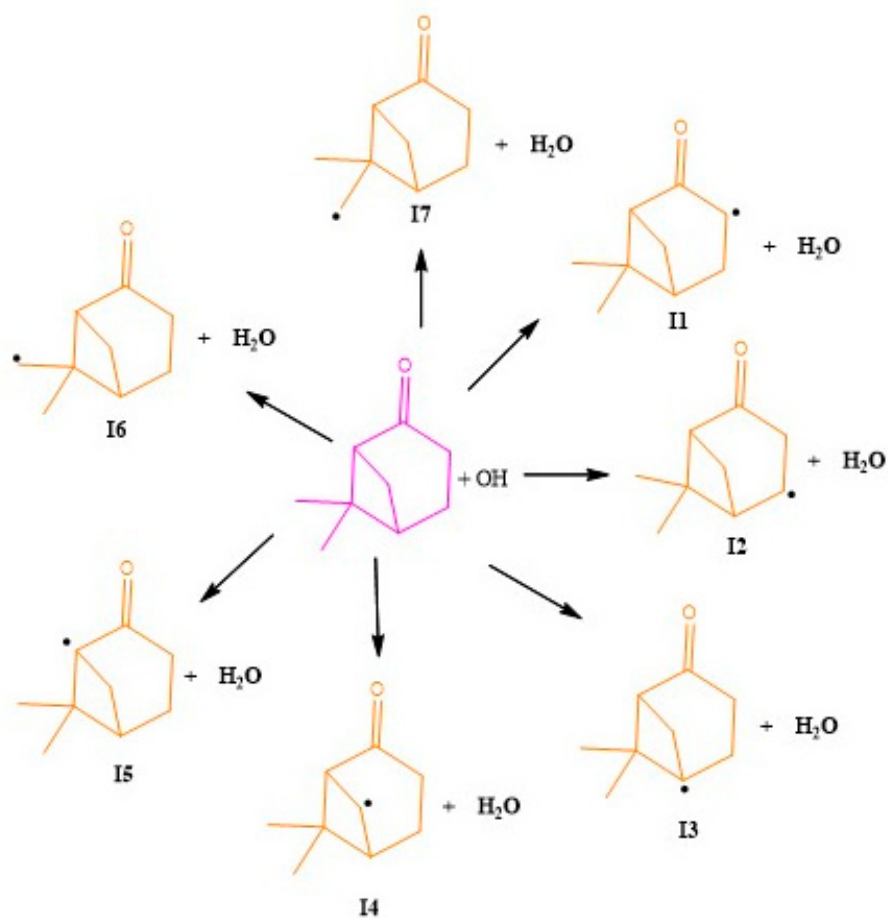


Figure 2. Plot of the pseudo-first-order decay rates as a function of the nopinone concentration. Experimental conditions: P = 80 Torr in argon; T = 298 K; [nopinone] = $(0.3\text{--}2.2) \times 10^{14} \text{ molecule cm}^{-3}$.

3.2. Theoretical Study

The structure of nopinone consists of different C–H bonds, and the oxidation of nopinone by OH radicals proceeds by the abstraction of H atoms from seven different reactive sites, from either $-\text{CH}$, $-\text{CH}_2$ or $-\text{CH}_3$ groups. The abstraction reaction pathways of nopinone with OH radicals were calculated using geometry optimization at the M06-2X/6-311++G(d,p) level of theory. The proposed initial H-atom abstraction reaction mechanism of nopinone with OH radicals is given in Scheme 2. The relative energy ΔE (kcal/mol), enthalpy ΔH (kcal/mol) and Gibbs free energy ΔG (kcal/mol) of the proposed H-atom abstraction reactions of nopinone with OH radicals calculated at the M06-2X/6-311++G(d,p) level of theory are given in Table 2. In addition to the initial reaction mechanism, we studied the subsequent secondary reaction mechanism of the most favourable pathway (Scheme S1). The values of the relative energy ΔE (kcal/mol), enthalpy ΔH (kcal/mol) and Gibbs free energy ΔG (kcal/mol) are tabulated in Table 3. The atom numbers are labelled and the optimized reactive species of all reactants (R), reactive complexes (RC), transition states, (TS) intermediate complexes (IC), intermediates (I) and products (P) of the initial and secondary reactions at the M06-2X level of theory with the 6-311++G(d,p) level of theory are given in the Supplementary Information (Figures S1 and S2). The initial reaction energy profiles of the H-atom abstraction pathways and those of the subsequent secondary reaction mechanisms calculated at the M06-2X/6-311++G(d,p) level of theory are given in Figures S3 and S4.



Scheme 2. Reaction scheme of the initial hydrogen abstraction reaction mechanism of nopinone by OH radicals.

Table 2. Relative energy, enthalpy, and Gibb's free energy (in kcal/mol) for the reaction of nopinone with OH radicals calculated at the M06-2X/6-311++g(d,p) level of theory.

Reaction Pathways		M06-2X/6-311++G(d,p)		
		ΔE	ΔH	ΔG
	R	0	0	0
PATHWAY 1	RC1	−9.41	−7.48	1.30
	TS1	−0.79	−2.13	7.34
	IC1	−36.13	−34.48	−26.75
	I1 + H ₂ O	−27.16	−27.90	−29.11
	TS2	1.37	0.06	8.44
PATHWAY 2	IC2	−27.18	−26.55	−20.06
	I2 + H ₂ O	−19.26	−20.62	−22.34
	TS3	1.12	0.02	8.10
PATHWAY 3	IC3	−21.67	−20.03	−12.85
	I3 + H ₂ O	−13.59	−13.92	−15.32
	TS4	2.26	0.71	9.38
PATHWAY 4	IC4	−23.43	−22.47	−15.30
	I4 + H ₂ O	−17.84	−16.53	−18.11

Table 2. Cont.

Reaction Pathways		M06-2X/6-311++G(d,p)		
		ΔE	ΔH	ΔG
PATHWAY 5	TS5	−1.23	−2.45	6.81
	IC5	−18.92	−17.10	−9.58
	I5 + H ₂ O	−10.61	−10.93	−12.38
PATHWAY 6	TS6	2.64	1.24	9.97
	IC6	−24.08	−23.41	−16.61
	I6 + H ₂ O	−15.80	−17.08	−18.53
PATHWAY 7	TS7	−0.95	−1.75	8.32
	IC7	−24.57	−23.62	−16.02
	I7 + H ₂ O	−16.13	−17.34	−18.95

Table 3. Relative energy, enthalpy and Gibb's free energy (in kcal/mol) for the reaction of the most favourable pathway with secondary atmospheric oxidants calculated at the M06-2X/6-311++g(d,p) level of theory.

Reaction Pathways		M06-2X/6-311++G(d,p)		
		ΔE	ΔH	ΔG
PATHWAY 8	I5 + O ₂	0	0	0
	I8	−43.39	−40.71	−35.54
PATHWAY 9	I8 + HO ₂	0	0	0
	TS8	35.40	34.68	32.71
	P1	−77.24	−75.93	−76.45
PATHWAY 10	I8 + NO	0	0	0
	I9	−63.79	−61.76	−61.27

It is well known from the initial reaction Scheme 1 that the H-atom abstraction pathways (1 to 7) take place from the C–H bond based on the -CH, -CH₂ and -CH₃ groups present in nopinone. Initially, the reactant (R) moves towards the pre-reactant complex (RC) through a barrierless reaction. The pre-reactant complexes (RCs) exhibit a hydrogen bond interaction between the H15 atom of the OH group and the O1 atom of nopinone, O2–H15•••O1, with a bond distance of 1.940 Å. As shown in Scheme 2, seven H-atom abstraction reactions occur from the C1 position to the C9 position. All seven H-atom abstraction reactions start from the RC complex and lead to intermediate complexes IC1 to IC7, along with the water molecule, through a transition state TS1 to TS7. Further, the reaction is transformed via TS to afford an intermediate complex formed by an intermolecular hydrogen bond and transformed into an intermediate (I1 to I7) along with a water molecule.

Initial H-atom abstraction from the -CH₂ group (Pathways 1, 2 and 4):

As shown in Scheme 1 and Table 2, Pathways 1, 2 and 4 take place through H-atom abstraction from the -CH₂ group located at the C6, C5 and C3 positions, respectively. Herein, we have shown that it is possible to characterize the potential energy surface of nopinone with OH radicals, in which the reaction Pathways 1, 2 and 4 take place via a H-atom abstraction reaction of the -CH₂ group via transition states TS1, TS2 and TS4, respectively, with an energy barrier of −0.79, 1.37 and 2.26 kcal/mol and an elongation of the C6–H8, C5–H6, and C3–H2 bonds in TS1, TS2 and TS4 by 1.183 Å, 1.153 Å and 1.163 Å, respectively; however, with respect to RC, the same C–H bond has bond distances of 1.090 Å, 1.092 Å and 1.092 Å, respectively. From Table 2, it is evident that all three

pathways (1, 2 and 4) are exothermic and exergonic, with reaction enthalpies (ΔH) and Gibbs free energies (ΔG) of -27.90 , -20.62 and -16.53 kcal/mol, and -29.11 , -22.34 and -18.11 kcal/mol, respectively. Based on the barrier heights of Pathways 1, 2 and 4, we found that Pathway 1 was the favourable pathway, with a small barrier height.

Initial H-atom abstraction from the -CH group (Pathways 3 and 5):

Pathways 3 and 5 correspond to H-atom abstraction from the C–H group, in which both the C4 and C2 positions of nopinone are attached to the C7 position, which carries two methyl groups. From Figure S1, the C4–H4 bond in TS3 has a bond distance of 1.149 Å with respect to the same bond in RC, which has a bond distance of 1.093 Å; hence, elongation of the bond takes place in TS3, which leads to the formation of intermediate I3 with an energy barrier of 1.12 kcal/mol. In Pathway 5, in the transition state (TS5) the C2–H1 bond is elongated, with a bond distance of 1.188 Å with respect to RC. The H1 atom is cleaved and abstracted by the OH radical, with a bond distance (H1●●●O2) of 1.351 Å. The product complex (PC1) is formed by means of an intermolecular hydrogen bond between O1–H15●●●O2, with a bond distance of 1.945 Å, and transformed into intermediate I5 along with a water molecule. Comparing both Pathways 3 and 5, it is well agreed by Table 2 that Pathway 5 is more favourable than Pathway 3, with an energy barrier of -1.23 kcal/mol. This may be due to the presence of carbon atom C6 situated at the four-membered ring, which is the bridge head position of nopinone. The reaction is exothermic and exergonic, with a reaction enthalpy and Gibbs free energy of -13.92 and -10.93 , and -15.32 and -12.38 kcal/mol, respectively.

Initial H-atom abstraction from the -CH₃ group (Pathways 6 and 7):

In Pathways 6 and 7, H-abstraction occurs on the -CH₃ group, in which the carbon atom is situated at the four-membered ring of nopinone with two methyl groups. From the above discussion, in the same manner, for the other pathways, Pathways 6 and 7 began with the reactant complex (RC) in transition states TS6 and TS7. The C9–H12 bond is cleaved, with a bond distance of 1.178 Å, and the H12 atom is abstracted by the OH radical, with a bond distance of 1.402 Å. Pathway 6 has an energy barrier of 2.64 kcal/mol, with a reaction enthalpy and Gibbs free energy of -17.08 and -18.53 kcal/mol, respectively. In Pathway 7, the C8–H10 bond is cleaved and O₂ abstracts the H10 atom, with a bond distance of 1.361 Å in transition state TS7 and a small energy barrier of -0.95 kcal/mol. The reaction is exothermic and exergonic, with enthalpy and Gibbs free energy of -17.34 and -18.95 kcal/mol, respectively.

Conclusively from the above discussion, from all the abstraction sites, Pathway 5 was found to be the most favourable reaction site, which had the bridge head position at C2 and a small barrier height. It is well agreed that, in the previous theoretical study of nopinone with OH radicals [11], the same reaction site remained the most favourable for reaction.

Secondary reaction mechanism of nopinone with OH radicals:

The optimized structure of the reactive species corresponding to the formation of secondary reactions of nopinone with OH radicals is shown in Figure S2.

The relative energy ΔE (kcal/mol), enthalpy ΔH (kcal/mol) and Gibbs free energy ΔG (kcal/mol) of the secondary reactions of nopinone were calculated at the M06-2X/6-311++G(d,p) level of theory. The obtained values are given in Table 3. Herein, the intermediate I5 reacts with O₂ to form a peroxy intermediate I8 (Pathway 8), as shown in Scheme 2. The formation of I8 (peroxy radical) is a barrierless reaction, reacting with atmospheric oxidants, such as HO₂ and NO radicals [27,28]. In Pathway 9, intermediate I8 reacts with the HO₂ radical, in which the reactants are transformed into product P1 through a transition state TS8, the H14 atom is abstracted by an O₃ atom with a bond distance of 1.547 Å and an energy barrier of 35.40 kcal/mol. The obtained product P1 (1-hydroperoxy-6,6-dimethylbicyclo [3.1.1] heptan-2-one) is exothermic and exergonic, with a reaction enthalpy and Gibbs free energy of -75.93 and -76.45 kcal/mol, respectively. I8 may react with NO (Pathway 10), leading to the formation of I9, in which the O₃ atom is abstracted by N1 in the form of a barrierless reaction. The expected products obtained from

the most favourable pathway in this study are the 1-peroxy-6,6-dimethylbicyclo [3.1.1] heptan-2-one radical and 1-hydroperoxy-6,6-dimethylbicyclo [3.1.1] heptan-2-one explored from the secondary atmospheric oxidants, O₂ and HO₂ radicals.

Kinetics of Nopinone with OH radicals:

The rate coefficient (cm³ molecule⁻¹ s⁻¹) for the most favourable pathway of nopinone with OH radicals calculated at the M06-2x/6-311++g(d,p) level of theory was calculated as a function of temperature in the range 278–350 K and is tabulated in Table 4. From the initial reaction mechanism, we found that Pathway 5 was the most favourable, with a small energy barrier. The rate coefficient of the H-atom abstraction reaction of Pathway 5 was found to be 2.21×10^{-11} cm³ molecule⁻¹ s⁻¹ at 298 K. The obtained theoretical rate coefficient agreed with our experimental value ($(1.74 \pm 0.35) \times 10^{-11}$ cm³ molecule⁻¹ s⁻¹). Figure 3 shows the temperature dependence of the rate coefficient of the reaction of nopinone with OH in the studied range of 278–350 K, where a negative temperature dependence is observed.

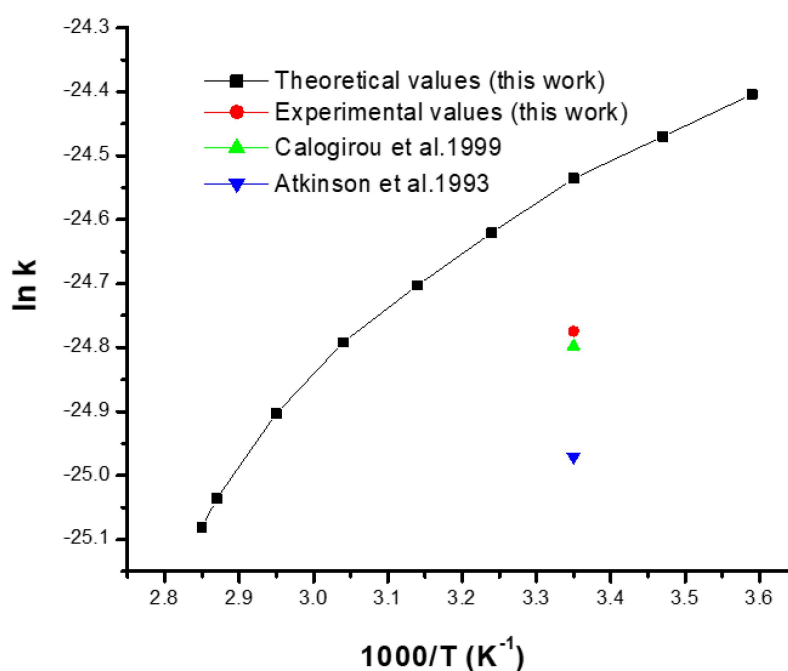


Figure 3. Theoretical and Experimental rate coefficients of the reaction of nopinone with OH radicals. —■— Theoretical values (this work) in the range of 278–350 K; —●— Experimental rate constant values (this work); —▲— Experimental rate constant obtained by Calogirou et al. (1999) [7]; —▼— Experimental rate constant obtained by Atkinson et al. (1993) [8].

Table 4. Rate coefficients (cm³ molecule⁻¹ s⁻¹) for the most favourable Pathway (I5) of nopinone with OH radicals calculated at the M06-2x/6-311++g(d,p) level of theory.

Temp (K)	K CVT/SCT (cm ³ molecule ⁻¹ s ⁻¹) × 10 ⁻¹¹
278	2.52
288	2.36
298	2.21
308	2.03
318	1.87
328	1.71

Table 4. *Cont.*

Temp (K)	K CVT/SCT ($\text{cm}^3 \text{ molecule}^{-1} \text{ s}^{-1}$) $\times 10^{-11}$
338	1.53
348	1.34
350	1.28

With respect to the current theoretical and experimental study, the rate coefficient was compared with previous theoretical studies found in the literature [11], in which the authors calculated the rate coefficient by using the transition state theory (TST) in the order of 10^{-12} magnitude at 298 K. Additionally, it is interesting to compare both TST and CVT method; hence, the CVT method gives more accurate results with respect to the small-curvature tunnelling method.

As mentioned before, little information exists in the literature on the reaction of nopinone with OH radicals. Atkinson and Aschmann [8] studied this reaction at room temperature and atmospheric pressure using the relative rate technique by gas chromatography with flame ionization detection (GC-FID). A rate coefficient of $(1.43 \pm 0.37) \times 10^{-11} \text{ cm}^3 \text{ molecule}^{-1} \text{ s}^{-1}$ was obtained using cyclohexane as a reference compound. The absolute rate coefficient of $(1.74 \pm 0.35) \times 10^{-11} \text{ cm}^3 \text{ molecule}^{-1} \text{ s}^{-1}$ obtained experimentally in this work at room temperature under the pressure range of 7–80 Torr is in good agreement with this value within experimental errors. Our value is also in good agreement with the unpublished value of $1.5 \times 10^{-11} \text{ cm}^3 \text{ molecule}^{-1} \text{ s}^{-1}$ provided by Hatakeyama et al. [9]. Since then, Calogirou et al. [7] studied the gas-phase reactions of nopinone with OH by a relative technique using Fourier transform infrared (FTIR) spectroscopy at room temperature and atmospheric pressure. A rate coefficient of $(1.7 \pm 0.2) \times 10^{-11} \text{ cm}^3 \text{ molecule}^{-1} \text{ s}^{-1}$ was found. Our experimental value is in excellent agreement with that provided by these authors.

4. Atmospheric Implications

The atmospheric lifetime of nopinone, due to the reaction with OH radicals, was calculated by using the formula below [29,30]:

$$\tau = \frac{1}{k[\text{OH}]} \quad (6)$$

where k denotes the rate coefficient of nopinone with OH radicals obtained in this work, and $[\text{OH}]$ refers to a 24 h daytime average global tropospheric OH radical concentration [31] of $1 \times 10^6 \text{ molecule cm}^{-3}$. Our experimental and theoretical values obtained upper lifetimes of 16 and 13 h, respectively. The reactivity of nopinone with OH radicals, NO_3 radicals and O_3 was investigated by Calogirou et al. [7], and lifetimes longer than 9 h, 47 days and 8 years were found due to reactions with OH, NO_3 and O_3 , respectively. To our knowledge, there are no data on other potential gas-phase removal pathways of nopinone, such as its reaction with Cl atoms and photolysis. These results confirm that nopinone is long-lived compared with the parent monoterpene β -pinene, for which a lifetime of 2.2 h with respect to OH is provided in the literature [8].

5. Conclusions

The kinetics of nopinone with OH radicals is studied via both experimental and theoretical methods. The results show that bridgehead position H-atom abstraction is the most favourable channel with a small barrier height. The obtained experimental rate coefficient is in good agreement with the theoretical value. In addition to the abstraction reaction mechanism, the OH addition mechanism is also possible for carbonyl compounds; hence, in the future, we plan to explore the addition mechanism of OH radicals with nopinone, and the overall rate constant as a function of temperature is currently being

explored in both theoretical and experimental studies. It is evident from the results obtained in this work and those available in the literature that the reaction with OH is a significant removal chemical process for nopinone in the gas phase in the atmosphere, showing that this process could play a role in the chemistry of the troposphere at the local scale. However, further work is needed to investigate the importance of other removal processes, mainly heterogenous losses.

Supplementary Materials: The following supporting information can be downloaded at: <https://www.mdpi.com/article/10.3390/atmos13081247/s1>, Figure S1 Optimized structure of the reactive species corresponding to the formation of initial H-atom abstraction reaction of nopinone with OH radical at M06-2X/6-311++G(d,p) level of theory. Figure S2 Optimized structure of the reactive species corresponding to the formation of secondary reactions of nopinone with OH radical at M06-2X/6-311++G(d,p) level of theory. Figure S3. Relative energy profile of initial H-atom abstraction reaction mechanism of nopinone by OH radical. Figure S4. Relative energy profile of secondary reactions of nopinone. Scheme S1. Reaction Scheme of secondary reactions of nopinone.

Author Contributions: Conceptualization, Data curation, Methodology, Formal analysis, Writing—review & editing, G.E.D. and A.M.P.; A.M.P.: Theoretical calculations and analysis; S.L.: Theoretical calculations and analysis; G.E.D. Supervised the work and writing of the manuscript; All authors discussed the results and commented on the manuscript. All authors have read and agreed to the published version of the manuscript.

Funding: This research was funded by INSU-LEFE CHAT French program.

Acknowledgments: The authors from Rennes gratefully thank the INSU-LEFE CHAT French program for financial support. The authors from India thank the University Grants Commission, New Delhi, India, for providing funds to establish High-Performance Computing facility, under the Center with Potential for Excellence in Particular Area (CPEPA) scheme (Grant 2-8/2016 (NS/PE), dated 3 October 2016).

Conflicts of Interest: The authors declare no conflict of interest.

References

1. Atkinson, R.; Arey, J. Gas-phase tropospheric chemistry of biogenic volatile organic compounds: A review. *Atmos. Environ.* **2003**, *37*, 197–219. [[CrossRef](#)]
2. Hoffmann, T.; Odum, J.R.; Bowman, F.; Collins, D.; Klockow, D.; Flagan, R.C.; Seinfeld, H.J. Formation of Organic Aerosols from the Oxidation of Biogenic Hydrocarbons. *J. Atmos. Chem.* **1997**, *26*, 189–222. [[CrossRef](#)]
3. Guenther, A.; Hewitt, C.N.; Erickson, D.; Fall, R.; Geron, C.; Graedel, T.; Harley, P.; Klinger, L.; Lerdau, M.; McKay, W.A.; et al. A global model of natural volatile organic compound emissions. *J. Geophys. Res. Atmos.* **1995**, *100*, 8873–8892. [[CrossRef](#)]
4. Sindelarova, K.; Granier, C.; Bouarar, I.; Guenther, A.; Tilmes, S.; Stavrou, T.; Müller, J.F.; Kuhn, U.; Stefani, P.; Knorr, W. Global data set of biogenic VOC emissions calculated by the MEGAN model over the last 30 years. *Atmos. Chem. Phys.* **2014**, *14*, 9317–9341. [[CrossRef](#)]
5. Hamilton, J.F.; Lewis, A.C.; Carey, T.J.; Wenger, J.C.; Garcia, E.B.i.; Muñoz, A. Reactive oxidation products promote secondary organic aerosol formation from green leaf volatiles. *Atmos. Chem. Phys.* **2009**, *9*, 3815–3823. [[CrossRef](#)]
6. Grossmann, D.; Moortgat, G.K.; Kibler, M.; Schlomski, S.; Bächmann, K.; Alicke, B.; Geyer, A.; Platt, U.; Hammer, M.-U.; Vogel, B.; et al. Hydrogen peroxide, organic peroxides, carbonyl compounds, and organic acids measured at Pabstthum during BERLIOZ. *J. Geophys. Res. Atmos.* **2003**, *108*, 001096. [[CrossRef](#)]
7. Calogirou, A.; Jensen, N.R.; Nielsen, C.J.; Kotzias, D.; Hjorth, J. Gas-Phase Reactions of Nopinone, 3-Isopropenyl-6-oxo-heptanal, and 5-Methyl-5-vinyltetrahydrofuran-2-ol with OH, NO₃, and Ozone. *Environ. Sci. Technol.* **1999**, *33*, 453–460. [[CrossRef](#)]
8. Atkinson, R.; Aschmann, S.M. Atmospheric chemistry of the monoterpene reaction products nopinone, camphenilone, and 4-acetyl-1-methylcyclohexene. *J. Atmos. Chem.* **1990**, *16*, 337–348. [[CrossRef](#)]
9. Hatakeyama, S.; Izumi, K.; Fukuyama, T.; Akimoto, H.; Washida, N. Reactions of OH with α -pinene and β -pinene in air: Estimate of global CO production from the atmospheric oxidation of terpenes. *J. Geophys. Res. Atmos.* **1991**, *96*, 947–958. [[CrossRef](#)]
10. Stolle, A. Synthesis of Nopinone from β -Pinene—A Journey Revisiting Methods for Oxidative Cleavage of C=C Bonds in Terpenoid Chemistry. *Eur. J. Org. Chem.* **2013**, *2013*, 2265–2278. [[CrossRef](#)]
11. Lewis, P.J.; Bennett, K.A.; Harvey, J.N. A computational study of the atmospheric oxidation of nopinone. *Phys. Chem. Chem. Phys.* **2005**, *7*, 1643–1649. [[CrossRef](#)] [[PubMed](#)]
12. Dib, G.E.; Azaad, B.; Lakshmi pathi, S.; Laversin, H.; Roth, E.; Chakir, A. An experimental and theoretical study on the kinetics of the reaction between 4-hydroxy-3-hexanone CH₃CH₂C(O)CH(OH)CH₂CH₃ and OH radicals. *Int. J. Chem. Kinet.* **2018**, *50*, 556–567. [[CrossRef](#)]

13. Priya, A.M.; Lakshmipathi, S.; Chakir, A.; El Dib, G. First Experimental and Theoretical Kinetic Study of the Reaction of 4-Hydroxy-4-methyl 2-pentanone as a Function of Temperature. *Int. J. Chem. Kinet.* **2016**, *48*, 584–600. [[CrossRef](#)]
14. Bouzidi, H.; Aslan, L.; El Dib, G.; Coddeville, P.; Fittschen, C.; Tomas, A. Investigation of the Gas-Phase Photolysis and Temperature-Dependent OH Reaction Kinetics of 4-Hydroxy-2-butanone. *Environ. Sci. Technol.* **2015**, *549*, 12178–12186. [[CrossRef](#)]
15. El Dib, G.; Sleiman, C.; Canosa, A.; Travers, D.; Courbe, J.; Sawaya, T.; Mokbel, I.; Chakir, A. First Experimental Determination of the Absolute Gas-Phase Rate Coefficient for the Reaction of OH with 4-Hydroxy-2-Butanone (4H2B) at 294 K by Vapor Pressure Measurements of 4H2B. *J. Phys. Chem. A* **2013**, *117*, 117–125. [[CrossRef](#)]
16. Zhao, Y.; Truhlar, D. The M06 suite of density functionals for main group thermochemistry, thermochemical kinetics, noncovalent interactions, excited states, and transition elements: Two new functionals and systematic testing of four M06-class functionals and 12 other functionals. *Theor. Chem. Acc.* **2008**, *120*, 215–241.
17. Zhao, Y.; Truhlar, D.G. Density Functionals with Broad Applicability in Chemistry. *Acc. Chem. Res.* **2008**, *41*, 157–167. [[CrossRef](#)]
18. Xie, H.-B.; Li, C.; He, N.; Wang, C.; Zhang, S.; Chen, J. Atmospheric Chemical Reactions of Monoethanolamine Initiated by OH Radical: Mechanistic and Kinetic Study. *Environ. Sci. Technol.* **2014**, *48*, 1700–1706. [[CrossRef](#)]
19. Arathala, P.; Musah, R.A. Computational Study Investigating the Atmospheric Oxidation Mechanism and Kinetics of Dipropyl Thiosulfinate Initiated by OH Radicals and the Fate of Propanethiyl Radical. *J. Phys. Chem. A* **2020**, *124*, 8292–8304. [[CrossRef](#)]
20. Gonzalez, C.; Schlegel, H.B. An improved algorithm for reaction path following. *J. Chem. Phys.* **1989**, *90*, 2154–2161. [[CrossRef](#)]
21. Gonzalez, C.; Schlegel, H.B. Reaction path following in mass-weighted internal. *Coord. J. Phys. Chem.* **1990**, *94*, 5523–5527. [[CrossRef](#)]
22. Garrett, B.C.; Truhlar, D.G. Generalized Transition State Theory. Bond Energy-Bond Order Method for Canonical Variational Calculations with Application to Hydrogen Atom Transfer Reactions. *J. Am. Chem. Soc.* **1979**, *101*, 4534–4548. [[CrossRef](#)]
23. Garrett, B.C.; Truhlar, D.G. Criterion of minimum state density in the transition state theory of bimolecular reactions. *J. Chem. Phys.* **1979**, *70*, 1593–1598. [[CrossRef](#)]
24. Garrett, B.C.; Truhlar, D.G.; Grev, R.S.; Magnuson, A.W. Improved treatment of threshold contributions in variational transition-state theory. *J. Phys. Chem.* **1980**, *84*, 1730–1748. [[CrossRef](#)]
25. Zheng, J.; Zhang, S.; Lynch, B.; Corchado, J.; Chuang, Y.; Fast, P.; Hu, W.; Liu, Y.; Lynch, G.; Nguyen, K. *Polyrate*; Version 2010-a; University of Minnesota: Minneapolis, MN, USA, 2010.
26. Frisch, M.J.; Trucks, G.; Schlegel, H.B.; Scuseria, G.; Robb, M.A.; Cheeseman, J.R.; Scalmani, G.; Barone, V.; Mennucci, B.; Petersson, G.A.; et al. *Gaussian 09*; Gaussian, Inc.: Wallingford, CT, USA, 2009.
27. Priya, A.M.; Lakshmipathi, S. DFT study on abstraction reaction mechanism of oh radical with 2-methoxyphenol. *J. Phys. Org. Chem.* **2017**, *30*, e3713. [[CrossRef](#)]
28. Priya, M.; Senthilkumar, L. Degradation of methyl salicylate through Cl initiated atmospheric oxidation—A theoretical study. *RSC Adv.* **2014**, *4*, 23464–23475. [[CrossRef](#)]
29. Kurylo, M.J.; Orkin, V.L. Determination of Atmospheric Lifetimes via the Measurement of OH Radical Kinetics. *Chem. Rev.* **2003**, *103*, 5049–5076. [[CrossRef](#)] [[PubMed](#)]
30. Arathala, P.; Musah, R.A. Thermochemistry and Kinetics of the Atmospheric Oxidation Reactions of Propanesulfinyl Chloride Initiated by OH Radicals: A Computational Approach. *J. Phys. Chem. A* **2022**, *126*, 4264–4276. [[CrossRef](#)] [[PubMed](#)]
31. Atkinson, R.; Baulch, D.L.; Cox, R.A.; Hampson, R.F., Jr.; Kerr, J.A.; Rossi, M.J.; Troe, J. Evaluated Kinetic and Photochemical Data for Atmospheric Chemistry: Supplement VI. IUPAC Subcommittee on Gas Kinetic Data Evaluation for Atmospheric Chemistry. *J. Phys. Chem. Ref. Data* **1997**, *26*, 1329–1499. [[CrossRef](#)]